GEOFYSISKE PUBLIKASJONER
GEOPHYSICA NORVEGICA
VOL. XXI NO. 6

CONTRIBUTION TO THE THEORY OF TWO-DIMENSIONAL MOUNTAIN WAVES

ENOK PALM AND ARNE FOLDVIK

FREMLAGT I VIDENSKAPS-AKADEMIETS MØTE DEN 11TE SEPTEMBER 1959

TRYKT MED BIDRAG FRA NORGES ALMENVITENSKAPELIGE FORSKNINGSRÅD

Summary. *a.* Mountain waves at high altitudes are studied in two models in order to examine the effect of these waves on the formation of mother of pearl clouds. It is found that with a mountain of height 700 m the maximum displacement at 20—30 km is about 400 m in both models and that the maximum vertical velocity in this region is 1 m sec^{-1} in one model and 3.5 m sec^{-1} in the other model.

b. The influence of wind and stability in the stratosphere on the wave motion in the lower troposphere is discussed. It is shown that if $f(z)$ (defined in the list of symbols) has a value at the ground which is at least 2.5 times as large as the minimum value of $f(z)$ (located at about 7—10 km above the ground), the wave motion in the lower troposphere is only depending on wind and stability beneath the level of minimum $f(z)$. This condition is usually satisfied when mountain waves occur.

c. For distributions of $f(z)$ fulfilling the requirement above, the motion near the ground may be obtained from a simple one-layer model. Such a model based on observed wind and stability is studied in section 5. A diagram is given from which the wave lengths are found directly without any computation. The drag on the mountain is computed in two cases. Non-linear effects are discussed, and the streamline field is found for three different mountains (Figs. 12, 14, 15) leading to motions with and without rotors depending on the height of the mountain. With the applied distribution of wind and stability, it is found that rotors occur when the mountain is higher than 600 m.

1. Introduction. It is a well known phenomenon that air passing over a mountain ridge will be set into oscillations if the air is sufficiently stable. These forced oscillations, usually denoted as lee waves or mountain waves, will in cases of large relative humidity be revealed in the form of lenticular clouds. If the amplitude of the mountain waves is large enough, a rotor cloud may be formed. In particular, lenticular clouds are frequently observed in mountainous countries.

Short review of earlier works. The contributions to the theory of two-dimensional mountain waves reviewed below are all based on linearized differential equations and

boundary conditions. These simplifications which obviously restrict the results obtained, will be discussed later in the present paper.

The theory of mountain waves may be traced back to works of RAYLEIGH (1883) and KELVIN (1886). They admittedly did not investigate waves in the atmosphere, but surface waves in a channel generated by a corrugation at the bottom. These problems are, however, in principle similar. The result obtained was that the disturbance of the free surface mainly consisted of one single harmonic wave.

The corresponding problem in the atmosphere, the mountain wave problem, was first investigated by LYRA (1943) and QUENEY (1947). In this case (see appendix 2 A) the motion depends on, besides the mountain profile, the variation with height of $f(z)$, defined in the list of symbols p. 29.

LYRA and QUENEY made the simplest possible assumption, considering $f(z)$ independent of height. The problem thereby was tractable from a mathematical point of view. With this assumption they found that the wave motion set up by a mountain did not consist of *one* single harmonic wave as in the case of a free surface, but of an integral of harmonic waves. The various waves interact and therefore cancel each other some distance from the mountain.

The streamline pattern found by LYRA and QUENEY obviously has many features consistent with observations. There is, however, also considerable deviations. Firstly, observations indicate a wave motion in the troposphere mainly composed of one (or a couple) harmonic wave, and not of a continuous spectrum of harmonic waves. Secondly, the LYRA-QUENEY model leads to too small amplitudes in the lower part of the troposphere.

It is readily seen from the soundings that the assumption of a constant value of $f(z)$ is a rather poor one. The variation of $f(z)$ with height was first taken into account by SCORER (1949) who considered a two-layer model with $f(z)$ constant in each layer. It turned out that if $f(z)$ was largest in the lowest layer, as usually observed when mountain waves occur, the motion in the model consisted principally of one harmonic wave component. Moreover, the amplitude in the troposphere was considerably larger than in the corresponding LYRA-QUENEY model.

Though this model is an improvement compared with the LYRA-QUENEY model, it is still a quite rough approximation to the atmosphere. Models consisting of more than two layers and with $f(z)$ varying within the layers consistent with observations have therefore been examined (WURTELE (1953), PALM (1958)). In the last-mentioned paper the results obtained by theory are compared with observations. The wave lengths were computed for two different distributions of $f(z)$, based on soundings obtained on days when the streamline pattern was observed. A good agreement was obtained.

In all the investigations mentioned above it is assumed that the motion is independent of time. This assumption simplifies the mathematical treatment considerably, but a logical difficulty is thereby introduced. It turns out, namely, that the motion in the stationary case is not uniquely determined by the boundary conditions at disposal.

Thus, from a mathematical point of view, it is impossible to decide whether the waves are located on the windward side or on the lee side of the mountain.

This ambiguity disappears, however, if the problem is solved as an initial value problem. This was shown by HØILAND (1952) for waves on a free surface and by WURTELE (1953) and PALM (1953) for the LYRA-QUENEY model.

It is found that, when time increases, the initial value solution approaches the stationary solution corresponding to waves on the lee side only. This result is easily generalized to comprise all cases where the group velocity is less than the phase velocity. This is the case in the present work and waves on the windward side are therefore excluded.

It should also be mentioned that the ambiguity discussed above may be removed in the LYRA-QUENEY model by introduction of a radiation condition (ELIASSEN and PALM (1954) or Handbuch der Physik, article on dynamic meteorology (1957)). This condition expresses the fact that in a frame of references where the mountain is moving the energy flux is directed away from the mountain.

Scope of the present work. The topic of this paper is divided into three parts which are more or less related:

a. Investigation of the motion at great heights (above 10 km, say).
b. Investigation of the influence of the distribution of wind and stability at great heights on the wave motion near the ground.
c. To demonstrate that the motion near the ground with a good approximation may be obtained from a one-layer model, to discuss non-linear effects and to examine the occurrence of rotor motion.

2. The differential equation and boundary conditions. Below, for simplicity, is only considered a motion independent of time. The flow takes place in a x-z plane with x-axis horizontal and z-axis positive upwards. $z = o$ corresponds to the ground. The equations and boundary conditions are for the present linearized. As to the boundary conditions, however, this assumption will be removed in section 5.

The density in the basic flow is assumed to be exponential in type[1]

$$\hat{\varrho} = \hat{\varrho}\,(o)\, e^{-\beta z} \qquad \beta > o \tag{2.1}$$

which is a close approximation to the variation of density in the atmosphere. The equation governing the motion is then found to be (see appendix 2 A)

$$\nabla^2 \omega + f(z)\,\omega = o \tag{2.2}$$

where ω and the other quantities are defined in the list of symbols.

Eq. (2.2) is most easily solved by applying FOURIER's theorem. Therefore, we first find the solution corresponding to a mountain profile

$$\zeta = a \cos kx \qquad \text{at } z = o \tag{2.3}$$

[1] For explanation see list of symbols on p. 29.

with a denoting a constant. Introducing that ω is a harmonic function of x, Eq. (2.2) takes the form

$$\omega_{zz} + (f(z) - k^2)\,\omega = 0. \tag{2.4}$$

The boundary conditions are

$$\begin{aligned} \omega &= U(0)\,\zeta_x = -\,a\,U(0)\,k\sin kx \qquad \text{at } z = 0 \\ \omega &= 0 \qquad\qquad\qquad\qquad\qquad\quad \text{at } z = \infty \end{aligned} \tag{2.5}$$

At the internal boundaries pressure and vertical velocity are required to be continuous.

3. On the wave motion at high altitudes. It is generally believed that the appearance of mother of pearl clouds is a manifestation of the existence of mountain waves at very great heights. Observations of these clouds seem to indicate a wave motion at about 20—30 km above sea-level with an apparent wave length of about 40 km (HESSTVEDT (1959), see also GEORGII(1956)). It ought to be pointed out that wave length in this connection is defined as the distance between consecutive clouds. To the authors' knowledge there are no observations which suggest the existence of a wave motion mainly consisting of one single harmonic wave.

In most models examined earlier $f(z)$ is assumed constant in the uppermost layer. This is an incorrect assumption in the present problem where emphasis is laid on the wave motion at high altitudes and thereby on relatively long waves. It may thus be demonstrated that by this assumption waves for which $k^2 < f^*$ (f^* the constant value of $f(z)$) are lost. As an example, if the layer is isothermal and the wind velocity 30 m sec^{-1}, the longest wave length attainable in the model is about 10 km. It should also be mentioned that with constant $f(z)$ in the uppermost layer, the amplitude of the wave motion tends towards infinity at great heights.

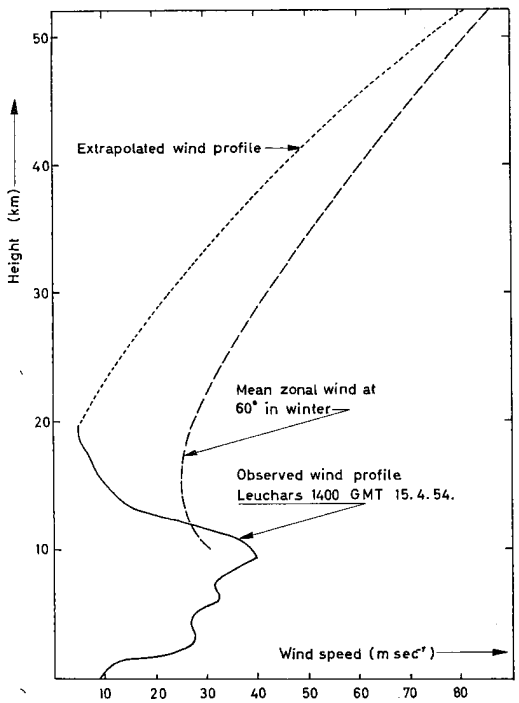

Figure 1. Observed wind, mean zonal wind at 60°N in winter and extrapolated wind profile.

It should be expected that the wave motion depends on the distribution of wind and stability from the ground and up to a height somewhat above the level in question. This complicates the present problem since simultaneous observations of wind and stability are not available up to these heights. We have therefore in this paper based the computations on the actual wind and sta-

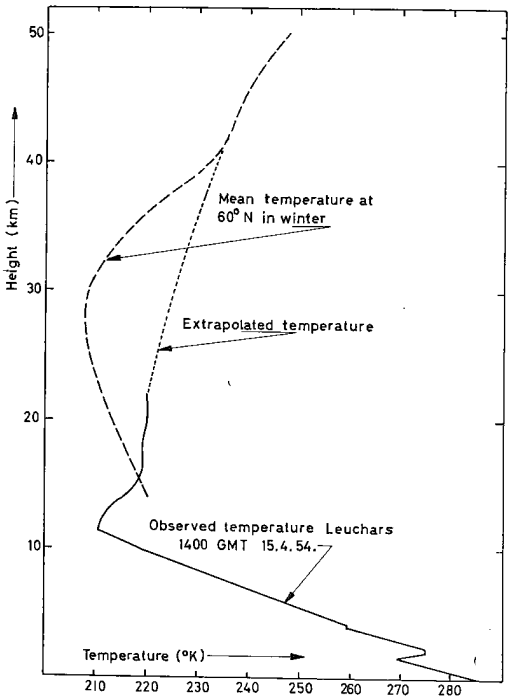

Figure 2. Observed temperature, mean temperature at 60°N in winter and extrapolated temperature.

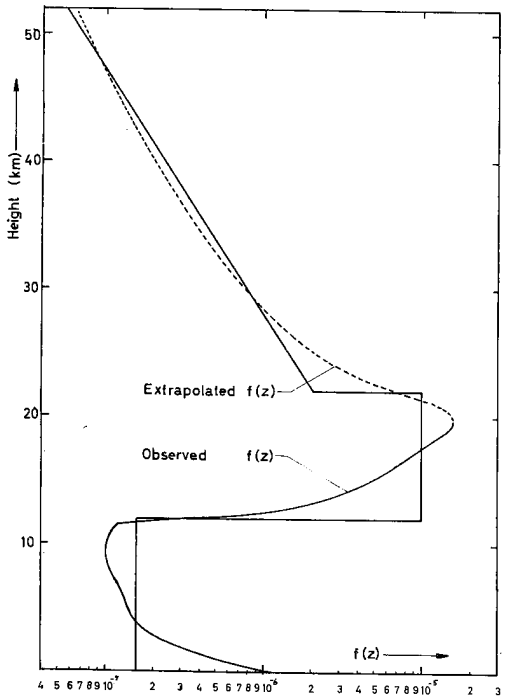

Figure 3. $f(z)$ computed from the observed and extrapolated wind and temperature given in Figs. 1 and 2, together with the simplified $f(z)$-curve applied in this section. Units: m^{-2}.

bility as far up as the soundings reach. Above this level the distribution of wind and stability is chosen consistent with the mean curves for the season. These curves are known to heights above 50 km.

Since we in this section will be particularly concerned with mountain waves at high altitudes, it would have been desirable to use a distribution of $f(z)$ obtained from soundings when mother of pearl clouds were observed. This is, however, not done here because, so far as we know, the soundings obtained in these situations only reached relatively moderate heights. The computations are based on observations at Leuchars 15.4.54 1400 GMT, a day on which the soundings reached a height of about 20 km. The observed wind, the mean wind distribution given by MURGATROYD (1957) and the extrapolated wind profile are displayed in Fig. 1. The corresponding curves for temperature are shown in Fig. 2. The resulting variation of $f(z)$ based on the observations and the extrapolated data are shown in Fig. 3 together with the simplified $f(z)$-curve applied here. By this simplification the model is divided into three layers with the following properties:

1. The first layer extends from the ground to $h_1 = 12$ km.
   $f(z) = f_1 = 1.6\ 10^{-7}\ m^{-2}$.

2. The second layer extends from 12 km to $h_2 = 22$ km.

   $f(z) = f_2 = 10^{-5}\, m^{-2}$.

3. The third layer extends from 22 km to infinity.

   $f(z)$ is given by

$$f(z) = f_3\, e^{-2c_3 z}$$

where $f_3 = 2.8\ 10^{-5}\, m^{-2}$ and $c_3 = 6.0\ 10^{-5}\, m^{-1}$.

The form of the exponent is chosen for later convenience.

The solution of Eq. (2.4) in the three layers are

$$\begin{aligned} \omega_1 &= A \sin \sqrt{f_1 - k^2}\, z + B \cos \sqrt{f_1 - k^2}\, z \\ \omega_2 &= C \sin \sqrt{f_2 - k^2}\, z + D \cos \sqrt{f_2 - k^2}\, z \\ \omega_3 &= E\, J_{\nu_3}(Z_3) \end{aligned} \tag{3.1}$$

with the boundary condition at infinity implied. A, B, C, D and E are arbitrary constants determined by the boundary conditions, $J_\nu(Z)$ denotes a Bessel function of the first kind and

$$\nu_3 = \frac{k}{c_3} \quad , \quad Z_3 = Z_3(z) = \frac{\sqrt{f_3}}{c_3}\, e^{-c_3 z} \quad .$$

The formula for ω corresponding to a symmetrical mountain is derived in the appendix (3 A). ω is adequately divided into two parts, here denoted by ω_r and ω_m. ω_r consists of a sum of harmonic lee waves and constitutes the real wave motion. It is seen that ω_r is zero for $z = o$ and discontinuous for $x = o$. Therefore, ω_m satisfies the boundary condition at $z = o$, and has the same kind of singularity as ω_r for $x = o$ in order to make the complete solution analytic. It is thus clear that ω_m is important near the mountain whereas it is readily shown that the importance of the term rapidly decreases for increasing distances from the mountain. In this and the next section this term is omitted, and the solution is therefore not valid near the mountain. In section 5, however, this term will be taken into account.

As shown in the appendix the harmonic waves composing ω_r have wave numbers which are the solutions of

$$\begin{aligned} &\left(J_{\nu_3}(\alpha_3) \cos \alpha_2 + \beta_2 J'_{\nu_3}(\alpha_3) \sin \alpha_2\right) \cos \alpha_1 \\ &- \beta_1 \left(J_{\nu_3}(\alpha_3) \sin \alpha_2 - \beta_2 J'_{\nu_3}(\alpha_3) \cos \alpha_2\right) \sin \alpha_1 = o. \end{aligned} \tag{3.2}$$

Here

$$\begin{aligned} &\alpha_1 = \sqrt{f_1 - k^2}\, h_1, \quad \alpha_2 = \sqrt{f_2 - k^2}\, (h_2 - h_1) \ , \quad \alpha_3 = Z(h_2) \ , \\ &\beta_1 = \frac{h_1 \alpha_2}{(h_2 - h_1)\, \alpha_1} \text{ and } \beta_2 = \frac{c_3 (h_2 - h_1) \alpha_3}{\alpha_2} \quad . \end{aligned} \tag{3.3}$$

Height (km)

Figure 4

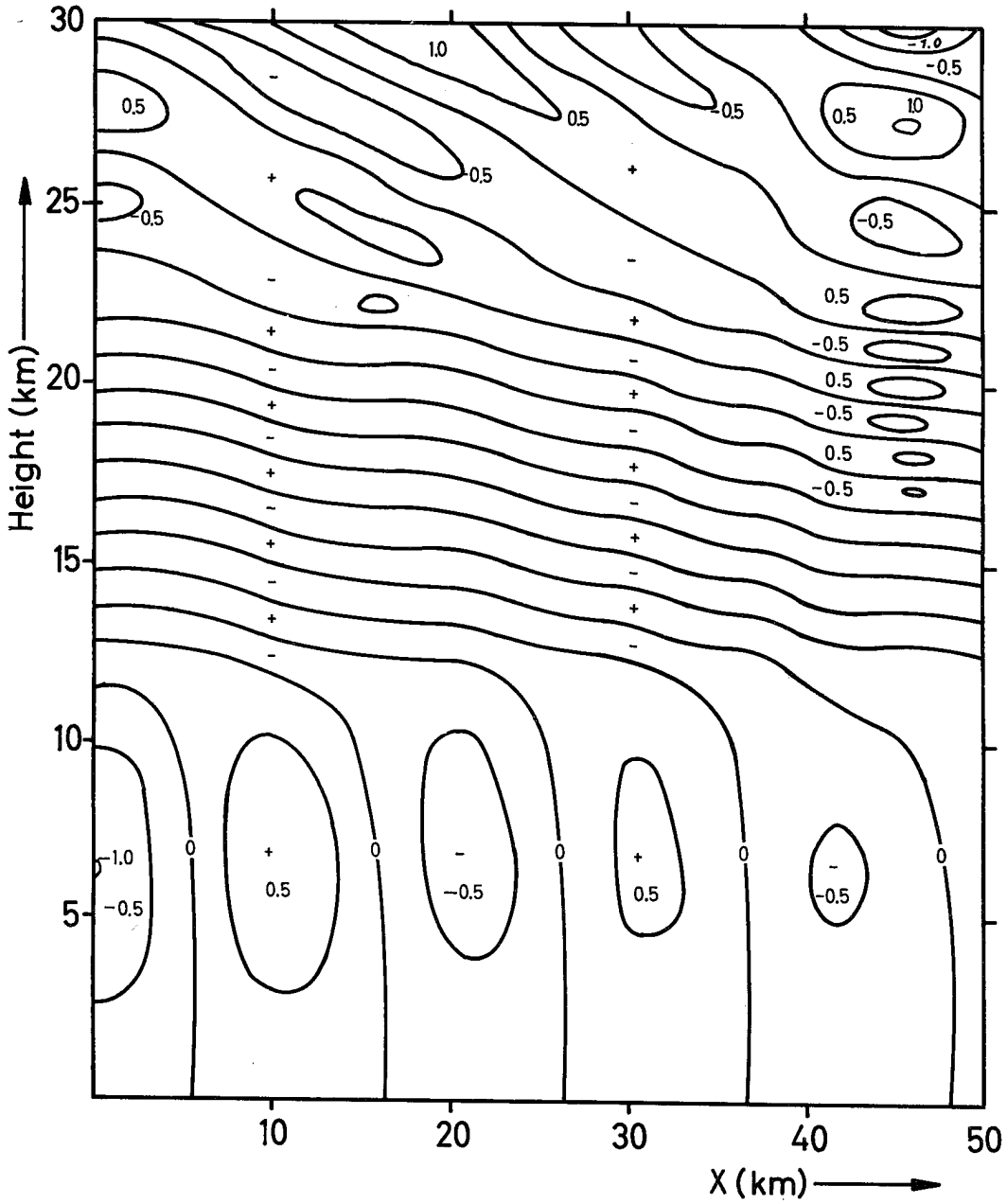

Figure 4. The field of vertical velocity due to a mountain of height 1 000 m applying linearized boundary conditions. Units: m sec^{-1}.

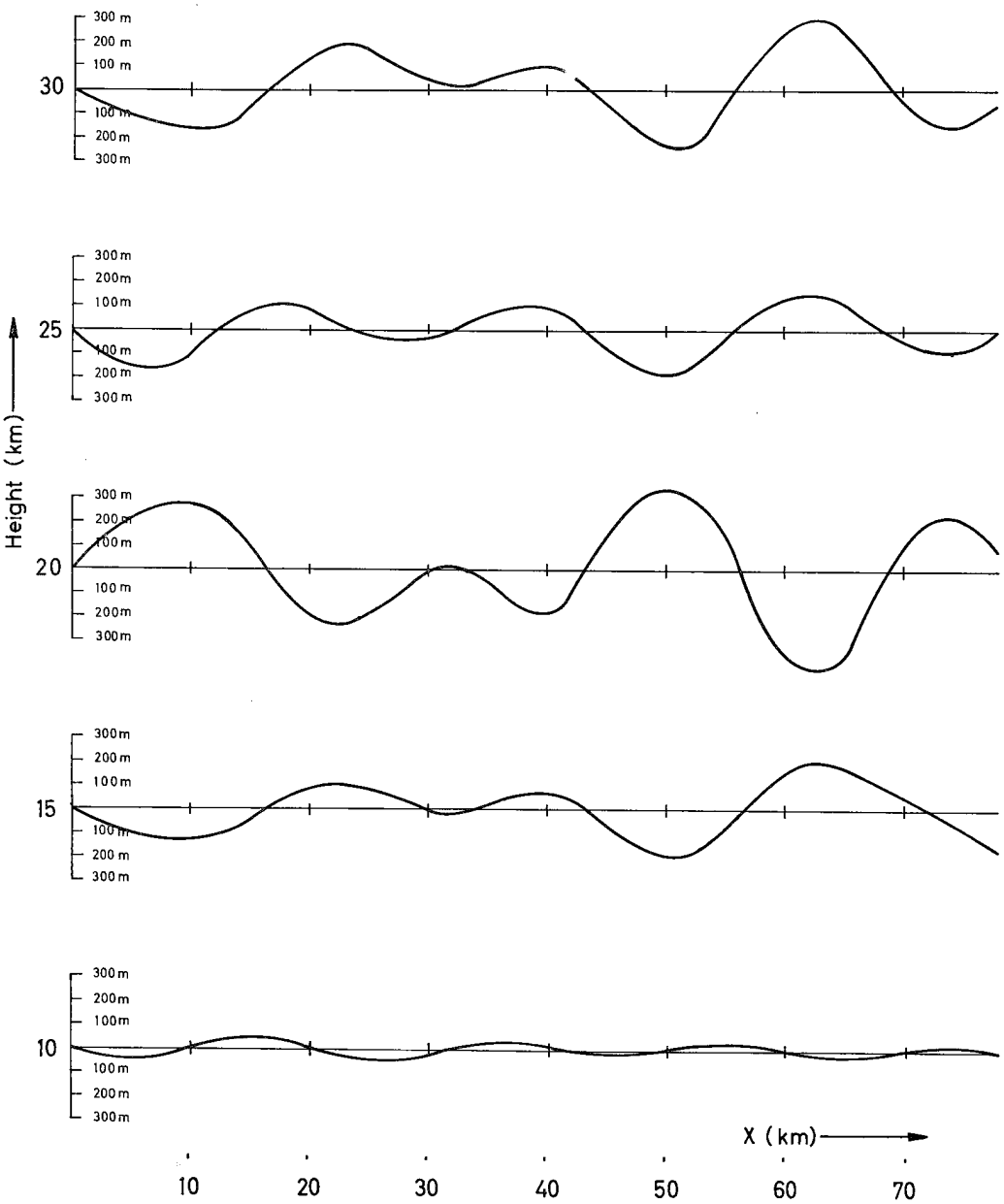

Figure 5. Streamlines due to a mountain of height 1 000 m applying linearized boundary conditions.

This equation yields 18 different wave numbers. The corresponding wave lengths are (in km):

37.0, 22.4, 19.0, 15.0, 10.4, 8.8, 7.0, 5.8, 4.9, 3.6, plus 8 solutions between 3.0 and 2.0 km.

The amplitudes of the wave components have been computed in the case of the symmetrical mountain profile

$$\zeta = \frac{H b^2}{x^2 + b^2} \tag{3.4}$$

where H, the height of the mountain, is 1 km and b, the half width, 2 km.

It is found that only the three longest waves have appreciable amplitude. The wave motion thus consists of three harmonic waves with wave lengths 37.0 km, 22.4 km and 19.0 km. All the waves omitted have wave numbers for which $k^2 > f_1$. It may be demonstrated that this is not a mere accident.

The vertical velocity field due to a mountain of form (3.4) is displayed in Fig. 4. The corresponding displacements of the streamlines at $z = 10$ km, 15 km, . . . 30 km are shown in Fig. 5. As seen in Fig. 4 the maximum vertical velocity in the troposphere is only about 1 m sec^{-1}. This is due to the choice of constant $f(z)$ in the troposphere. If the observed variation of $f(z)$ is taken into account, as done in section 5, the vertical velocity will be considerably larger.

It is seen that the two shortest waves dominate near the ground whereas all three wave components are important aloft. Here the three waves interact, reinforcing and cancelling each other. Thus at an altitude of 20 km these three waves lead to a wave motion with an apparent wave length of about 40 km which is the wave length indicated by observations of mother of pearl clouds. The maximum displacement at this level is about 350 m, leading to a cooling of the ascending air of 3.5°C. By more suitable distributions of wind and stability than that discussed here, the cooling of the air may be considerably larger. It therefore seems reasonable that mountain waves may be of importance for the formation of mother of pearl clouds.

It is noted that from 12 km to 22 km the vertical velocity is zero on lines spaced at about 1 km in the vertical direction. This is due to the small wind velocity and large stability at these heights, leading to a large $f(z)$. Above this layer the maximum vertical velocity increases with height being about 1 m sec^{-1} at 30 km.

It seems difficult to decide at which height the result obtained ceases to be valid. Evidently friction and three-dimensional effects play a dominant rôle at very great heights.

An inspection of Eq. (3.2) reveals that all three waves, and therefore also the wave motion near the ground, are considerably dependent on wind and stability at high levels. In the next section, however, the variation of $f(z)$ with height in the troposphere is taken into account. It is then shown that for variations of $f(z)$ as usually observed when mountain waves occur, the wave motion in the lower troposphere is independent of wind and stability aloft.

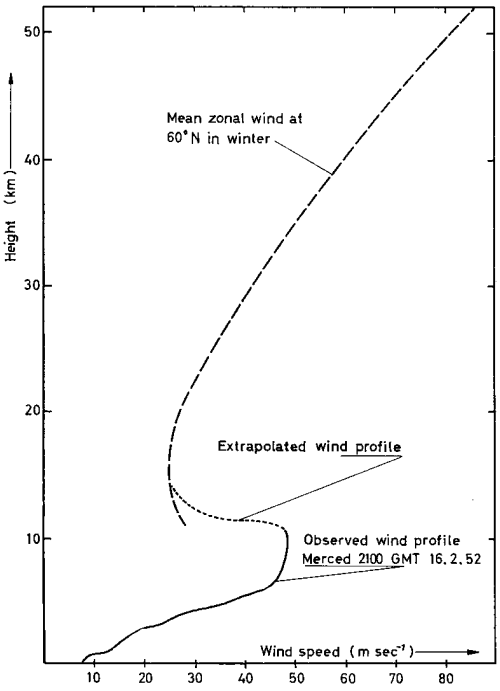

Figure 6. Observed wind, mean zonal wind at 60°N in winter and extrapolated wind profile.

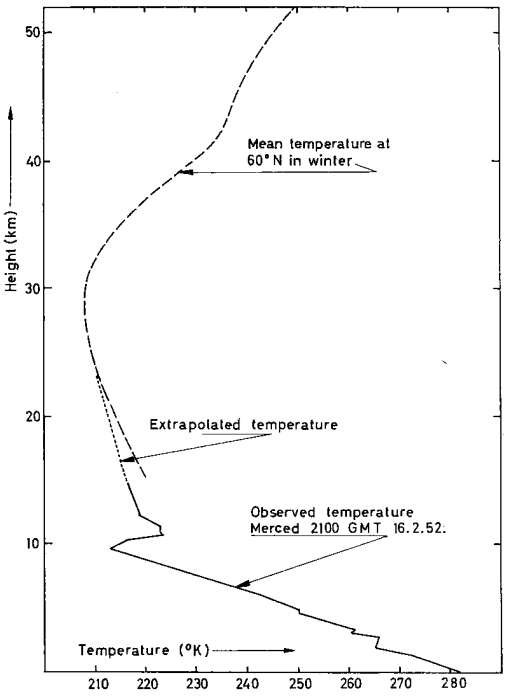

Figure 7. Observed temperature, mean temperature at 60°N in winter and extrapolated temperature.

4. On the connection between the motion near the ground and the wind and stability aloft. An examination of $f(z)$-curves based on soundings on days when mountain waves were observed reveals a characteristic variation with height. In the lower troposphere $f(z)$ decreases up to an altitude corresponding approximately to maximum wind velocity. Here the function is relatively small in a 2—3 km thick layer, and then it starts to increase rapidly. Often this characteristic distribution of $f(z)$ is camouflaged by abrupt, concentrated changes of the function mainly due to thin inversion layers.

The purpose of this section is to demonstrate that for variations of $f(z)$ as sketched above, the distribution of wind and stability above the level of minimum $f(z)$ does not sensibly influence the motion beneath this level. The model to be studied in this section might have been based on the observations displayed in the previous section. We have, however, here preferred to found the model on a sounding launched on February 16, 1952 in the Sierra Nevada region (HOLMBOE and KLIEFORTH (1957)). The wind profile was only obtained to a height of about 11 km, but, on the other hand, on that day the streamline field was carefully observed by a glider. Besides that, a rotor motion occurred. This will be of interest in the next section where the complete streamline field will be computed and special emphasis laid on the rotor phenomenon.

The observed values of wind and temperature are displayed in Figs. 6 and 7, respectively. On the same figures are also shown the mean distributions of wind and temperature above 11 km at 60°N in winter as given by MURGATROYD (1957). The resulting variation of $f(z)$ based on the observations and mean data are shown in Fig. 8 together with the simplified variation of $f(z)$ applied in this section.

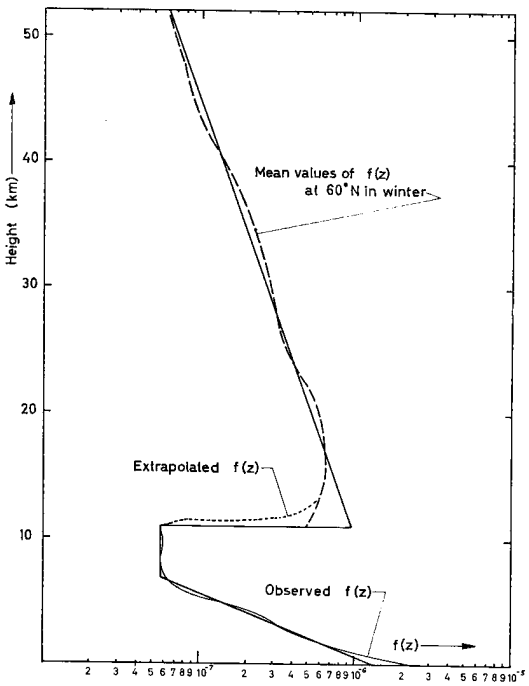

Figure 8. $f(z)$ computed from the observed, extrapolated and mean values of wind and temperature given in Figs. 6 and 7, together with the simplified $f(z)$-curve applied in this section. Units: m^{-2}.

It is seen from Fig. 8 that the actual model is divided into three layers with the following properties:

1. The first layer extends from the ground to $h_1 = 7$ km.

   $f(z)$ is given by

   $$f(z) = f_1 e^{-2c_1 z}$$

   where $f_1 = 1.3\ 10^{-6}\ m^{-2}$ and $c_1 = 2.3\ 10^{-4}\ m^{-1}$.

2. The second layer extends from 7 km to $h_2 = 11$ km.

   $f(z) = f_2 = 5.8\ 10^{-8} m^{-2}$.

3. The third layer extends from 11 km to infinity.

   $f(z)$ is given by

   $$f(z) = f_3\, e^{-2c_3 z}$$

   where $f_3 = 2.0\ 10^{-6} m^{-2}$ and $c_3 = 3.4\ 10^{-5} m^{-1}$.

The solutions of (2.4) in the three layers are

$$\omega_1 = A\,\mathcal{J}_{\nu_1}(\mathcal{Z}_1) + B N_{\nu_1}(\mathcal{Z}_1)$$

$$\omega_2 = C \sin \sqrt{f_2 - k^2}\, z + D \cos \sqrt{f_2 - k^2}\, z \tag{4.1}$$

$$\omega_3 = E\,\mathcal{J}_{\nu_3}(\mathcal{Z}_3)$$

where the boundary condition at infinity is implied. Here $\mathcal{J}_\nu$ and N_ν are Bessel functions of the first and second kind, respectively, and

$$\nu_1 = \frac{k}{c_1} \qquad Z_1 = Z_1(z) = \frac{\sqrt{f_1}}{c_1} e^{-c_1 z}$$
$$\nu_3 = \frac{k}{c_3} \qquad Z_3 = Z_3(z) = \frac{\sqrt{f_3}}{c_3} e^{-c_3 z} \quad . \tag{4.2}$$

A, B, C, D and E are arbitrary constants determined by the boundary conditions.

The formula for ω corresponding to a symmetrical mountain is derived in the appendix (4 A). The wave numbers of the harmonic waves composing ω_r are found to be solutions of

$$\mu_1 \left(- \mathcal{J}_{\nu_3}(\lambda_3) \sin \lambda_2 + \mu_2 \mathcal{J}'_{\nu_3}(\lambda_3) \cos \lambda_2 \right) \left(\mathcal{J}_{\nu_1}(\lambda_0) N_{\nu_1}(\lambda_1) - \mathcal{J}_{\nu_1}(\lambda_1) N_{\nu_1}(\lambda_0) \right)$$
$$- \left(\mathcal{J}_{\nu_3}(\lambda_3) \cos \lambda_2 + \mu_2 \mathcal{J}'_{\nu_3}(\lambda_3) \sin \lambda_2 \right) \left(\mathcal{J}_{\nu_1}(\lambda_0) N'_{\nu_1}(\lambda_1) - \mathcal{J}'_{\nu_1}(\lambda_1) N_{\nu_1}(\lambda_0) \right) = 0. \tag{4.3}$$

Here

$$\lambda_0 = Z_1(o) \ , \ \lambda_1 = Z_1 \ (h_1) \ , \ \lambda_2 = \sqrt{f_2 - k^2} \ (h_2 - h_1) \ ,$$
$$\lambda_3 = Z_3 \ (h_2) \ , \ \mu_1 = \frac{\lambda_2}{c_1(h_2 - h_1)\lambda_1} \text{ and } \mu_2 = \frac{c_3(h_2 - h_1)\lambda_3}{\lambda_2} \quad . \tag{4.4}$$

Eq. (4.3) is solved graphically and yields 9 different wave numbers. The corresponding wave lengths are (in km)

45.5, 29.4, 21.7, 16.6, 14.4, 13.6, 11.2, 9.3, 7.7. (4.5)

For the two longest waves $k^2 < f_2$ whereas for the other waves $k^2 > f_2$.

Most of these waves have very small amplitudes in the lowest layer. It is shown in the appendix (4 B) that, retaining only waves of appreciable amplitudes, the complicated Eq. (4.3) reduces for $k^2 > f_2$ and $f_1 > 2.5 f_2$ to

$$\mathcal{J}_{\nu_1}(\lambda_0) = 0. \tag{4.6}$$

In the actual case $f_1 = 25 f_2$ and, therefore, for $k^2 > f_2$ (here corresponding to wave lengths less than 25 km) the motion near the ground is independent of the parameters in the upper layer. Eq. (4.6) has few solutions compared with (4.3), in the actual case only one corresponding to the wave length 14.4 km.

It does not seem possible to reduce Eq. (4.3) for $k^2 < f_2$. Examples indicate, however, that generally the amplitudes of these waves are small below the level of minimum $f(z)$. This is true in the present case, as seen from Fig. 9. The vertical velocity field displayed in this figure is due to a mountain of form (3.4) and is computed from the complete set of equations. The figure reveals clearly that only the wave of wave length 14.4 km is important in the lowest layer.

It is seen that the maximum vertical velocity is about 6 m sec^{-1} and is located below 5 km. This value is considerably larger than that found in the previous section. This is due to the decrease of $f(z)$ with height in the lowest troposphere incorporated in this model. Also at higher altitudes the vertical velocity in the present model is larger than

Figure 9 condition

Height (km)

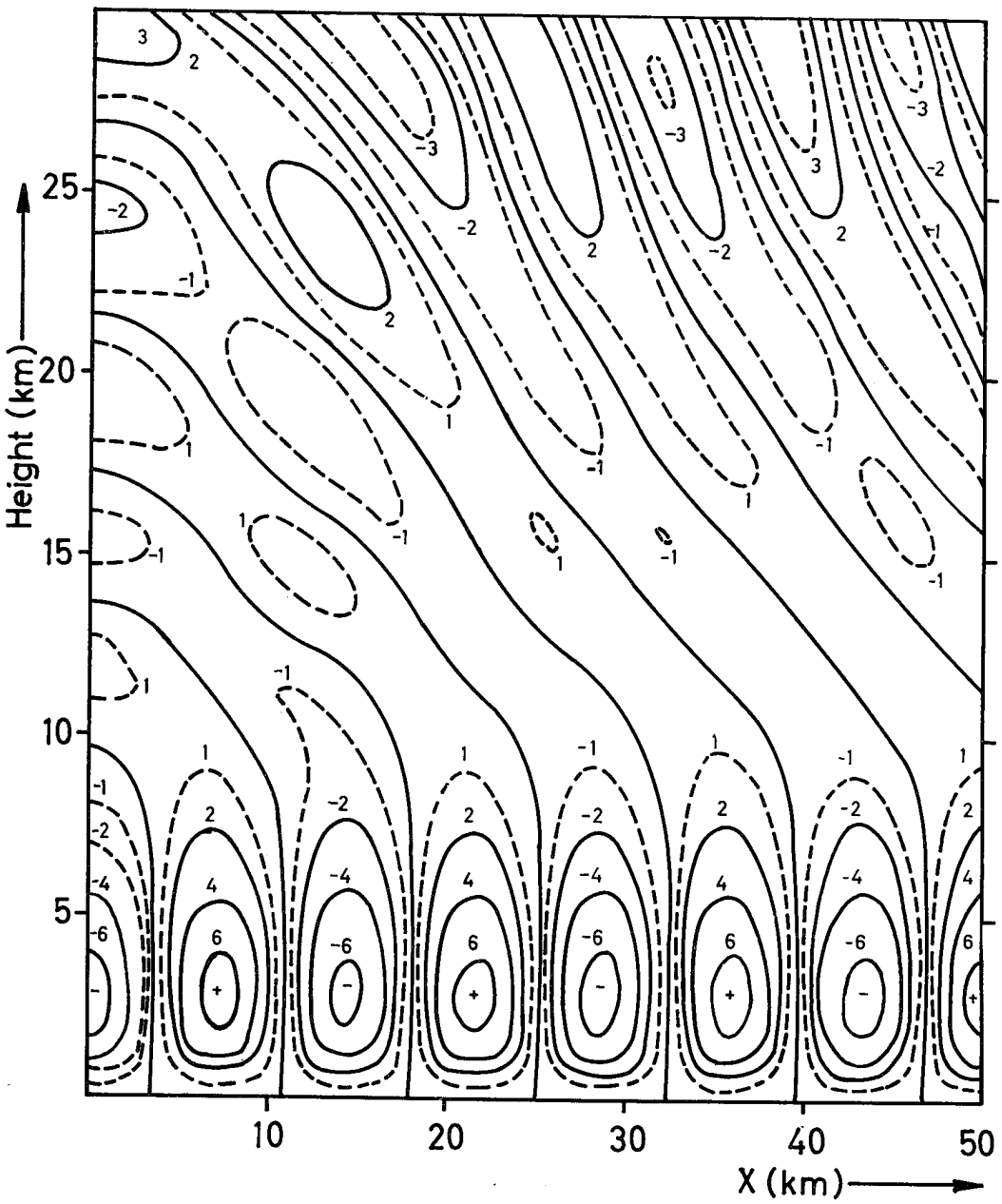

Figure 9. The field of vertical velocity due to a mountain of height 1 000 m applying linearized boundary conditions, or, according to section 5, due to a mountain of height 700 m applying the correct boundary conditions. Units: m sec^{-1}.

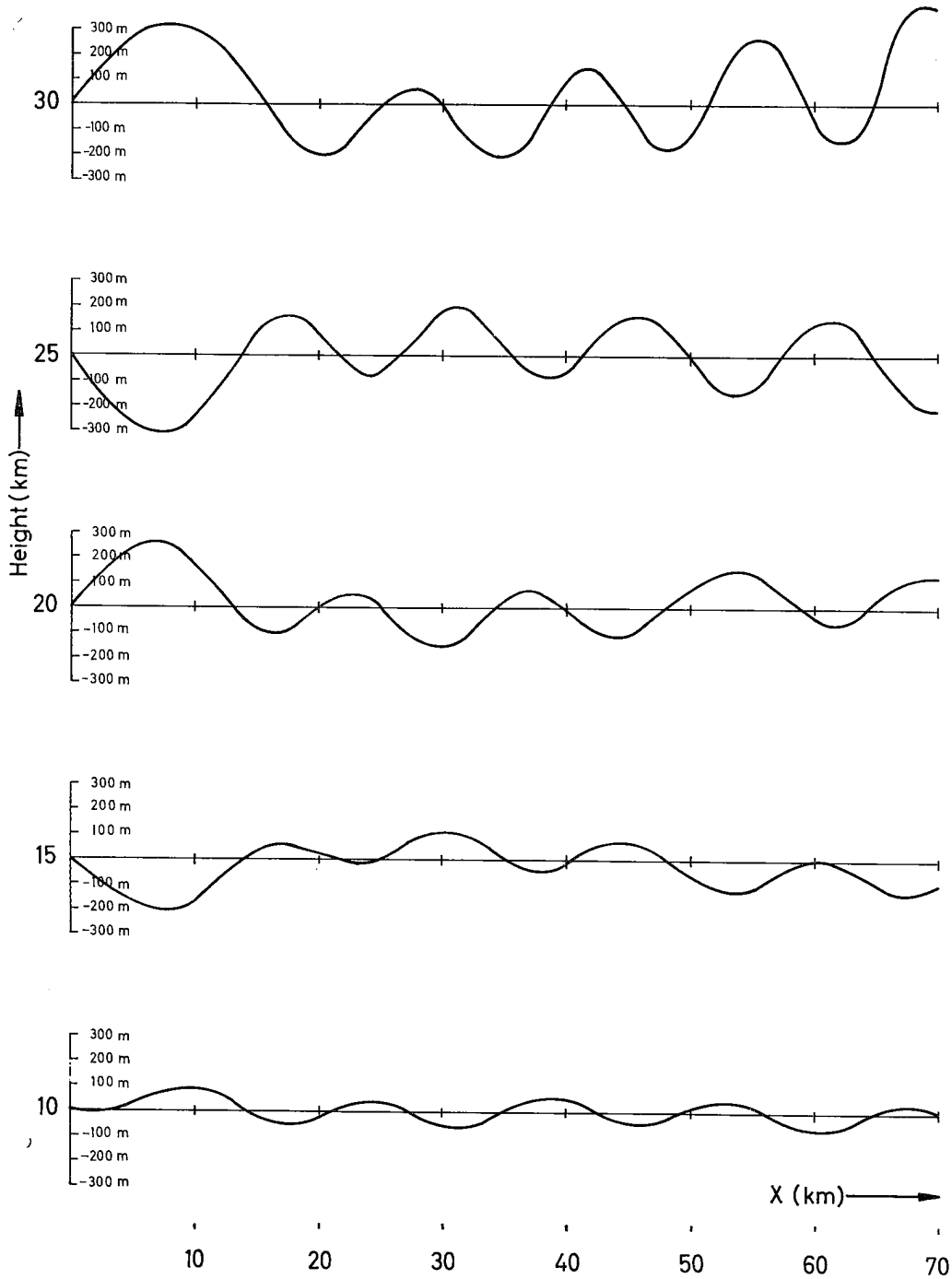

Figure 10. Streamlines due to a mountain of height 1 000 m applying linearized boundary conditions, or, according to section 5, due to a mountain of height 700 m applying the correct boundary conditions.

in the previous one. For example, at 30 km the vertical velocity in the actual case is found to be about 3.5 m sec^{-1}. The field of vertical velocity between 12 km and 22 km has a different pattern in Figs. 4 and 9 due to widely differing values of $f(z)$ in this region.

The displacement of the streamlines at $z = 10$ km, 15 km, . . . 30 km are shown in Fig. 10. It is seen that the displacement at 30 km is about 400 m.

Eq. (4.6) is identical with the equation found in a one-layer model with $f(z)$ decreasing exponentially with height. Consequently, the wave motion in the lower troposphere may be obtained from a simple one-layer model. This model is tractable from a mathematical point of view and will be discussed in the next section.

5. The motion near the ground. Neglecting subscripts $f(z)$ is now in the entire atmosphere given by

$$f(z) = f(o)e^{-2cz} \tag{5.1}$$

or, for later convenience,

$$lnf(z) = lnf(o) - 2cz. \tag{5.2}$$

It follows from the appendix (4 A) that in the case of a mountain of form (3.4) with H and b arbitrary,

$$\left.\begin{aligned} \omega_m &= Hb\,U(o)\,I\int_0^\infty ke^{-ikb}\frac{\mathcal{J}_{iv}(\mathcal{Z})}{\mathcal{J}_{iv}(\lambda_0)}e^{-kx}\,dk \\ \omega_r &= -2\pi Hb\,U(o)\sum_k k\,e^{-kb}\frac{\mathcal{J}_v(\mathcal{Z})}{\frac{d}{dk}\mathcal{J}_v(\lambda_0)}\cos kx \end{aligned}\right\} x > o \tag{5.3}$$

and

$$\left.\begin{aligned} \omega_m &= -Hb\,U(o)\,I\int_0^\infty ke^{-ikb}\frac{\mathcal{J}_{iv}(\mathcal{Z})}{\mathcal{J}_{iv}(\lambda_0)}e^{kx}dk \\ \omega_r &= o\,, \end{aligned}\right\} x < o \tag{5.4}$$

where I denotes the imaginary part. Here

$$\nu = \frac{k}{c} \qquad \mathcal{Z} = \mathcal{Z}(z) = \frac{\sqrt{f}}{c}e^{-cz}\,. \tag{5.5}$$

The waves composing the sum in (5.3) are the solutions of

$$\mathcal{J}_\nu(\lambda_0) = o\,. \tag{5.6}$$

The solutions of (5.6) are easily obtained from the diagram in Fig. 11 derived from tables of Bessel functions. In this figure $f(o)$ and c are the coordinates. The solid lines and dashed lines are isolines of constant wave length. Thus for large c-values and small $f(o)$-values no solution exists. For smaller c-values or larger $f(o)$-values one solution

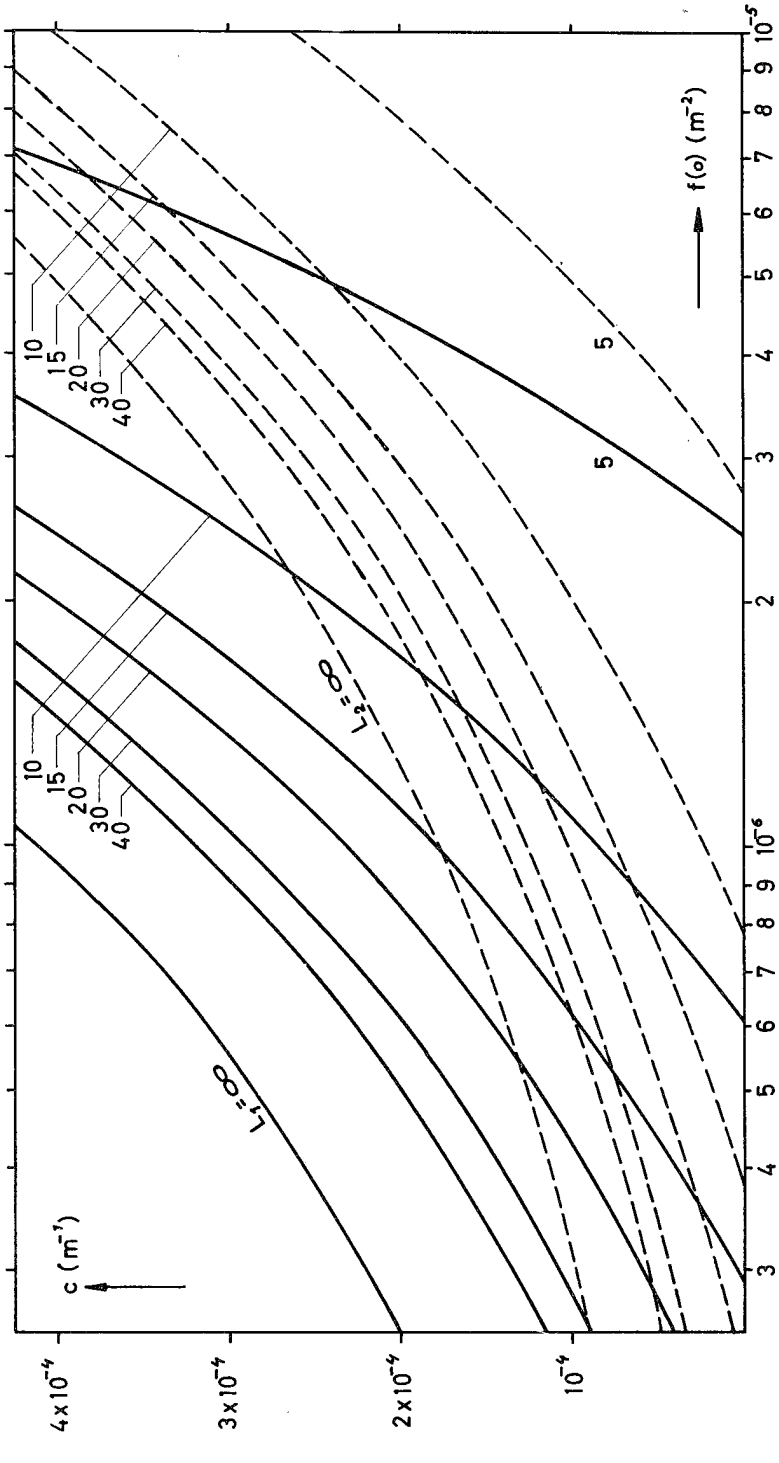

Figure 11. The wave lengths corresponding to observed $f(o)$ and c are found directly from the diagram. If the point $(f(o), c)$ lies to the left of $L_1 = \infty$ no wave exists, between $L_1 = \infty$ and $L_2 = \infty$ one wave exists, and to the right of $L_2 = \infty$, two waves exist. The numbers attached to the lines denote the wave length in km.

(wave) exists. For still smaller c-values or larger $f(o)$-values two solutions exist. More than the two sets of curves shown on the diagram could have been drawn, leading to the possibility of three or more solutions of (5.6). This is not done here because these sets of curves correspond to unrealistic values of wind and stability. When applying this diagram, it should be kept in mind that only waves for which $f_1 > 2.5 f_2$ and $k^2 > f_2$ should be taken into account. f_2 denotes as above the observed minimum value of $f(z)$ corresponding approximately to maximum wind velocity.

The possible wave lengths are therefore found by the following procedure. $ln\, f(z)$ is plotted from 1 km, say, (to avoid the friction layer) and up to the level where $f(z)$ has its minimum value, f_2. The straight line is drawn which fits the plotted points best. Thereby, from (5.2) $f(o)$ and c are found. The corresponding wave lengths are obtained from the diagram in Fig. 11. Only wave numbers for which $k^2 > f_2$ should be taken into account.

The drag on the mountain. The total drag of the air on the mountain is obtained by integrating the momentum transport along the x-axis. For a symmetrical mountain

$$\text{Drag} = -\int_{-\infty}^{\infty} \hat{\varrho}\, uw\, dx = -\hat{\varrho}\int_{0}^{\infty} u_r\, w_m\, dx \qquad \text{for } z = o \tag{5.7}$$

where subscripts r and m are used in the corresponding meaning as above. Introduction of the expressions for u_r and w_m leads in the case of a mountain of form (3.4) to

$$\text{Drag} = -\hat{\varrho}\, A \int_{0}^{\infty} \frac{x}{(b^2 + x^2)^2} \sin kx\, dx \tag{5.8}$$

where

$$A = 4\pi H^2 b^3 U^2(o)\, c^2 e^{-kb}\, \lambda_0 \frac{\mathcal{J}'_\nu(\lambda_0)}{\frac{d}{d\nu}\mathcal{J}_\nu(\lambda_0)} \tag{5.9}$$

A prime denotes differentiation with respect to the argument. Evaluation of the integral (5.8) leads to

$$\text{Drag} = -\hat{\varrho}\, A \frac{k\pi}{4b} e^{-kb} \tag{5.10}$$

Introducing $U(o) = 10$ m sec^{-1}, $H = 1$ km, $b = 2$ km and $f(o) = f_1$, $c = c_1$ (f_1 and c_1 given in section 4) the drag is 8.8 10^7 dyne cm^{-1}. If $H = 0.5$ km and $b = 2$ km the drag is found to be 2.2 10^7dyne cm^{-1}.

For comparison, SAWYER (1959) applying the Lyra-Queney model with $U(o) = 20$ m sec^{-1}, $H = 0.3$ km and $b = 2$ km, found that the drag was 7.6 10^6 dyne cm^{-1}.

The non-linear effects. The results obtained above are based on boundary conditions and differential equations which are linearized. This, of course, restricts the validity of the solution. For the motion near the ground especially the linearization of the

boundary conditions may lead to fallacious results. This approximation is avoided by considering the linearized solution as the motion generated by a mountain profile coinciding with one of the streamlines. In order to obtain a mountain profile consisting of one single ridge, it is usually necessary (but not sufficient) to choose the streamline approaching the ground far upstream. Various mountain profiles are obtained by varying the linearized boundary conditions. This method, introduced by LONG (1955) in this kind of problem, will be applied below.

The non-linear equation governing the motion in the case of an incompressible fluid may be written (LONG 1953)

$$\nabla^2\zeta + \frac{1}{2}\frac{d}{dz_0} ln \left(U^2(z_0)\,\hat{\varrho}\,(z_0)\right)\left((\nabla\zeta)^2 + 2\frac{\partial\zeta}{\partial z}\right) = -\frac{S(z_0)}{U^2(z_0)}\,\zeta \quad . \tag{5.11}$$

Here

$$S(z_0) = -\frac{g}{\hat{\varrho}}\frac{d\hat{\varrho}}{dz_0} \quad ,$$

ζ the vertical displacement of a streamline and z_0 the z-coordinate far upstream. If compressibility is taken into account, the equation corresponding to (5.11) will be considerably complicated. For the present purpose, however, it is sufficient to consider the influence of compressibility on the stability term only, which is the most important effect. The equation for finite amplitude then takes the form (5.11) with

$$S(z_0) = \frac{g(\gamma_d - \gamma)}{T} \quad , \tag{5.12}$$

implied that γ is the lapse rate far upstream.

The linearized equation corresponding to (5.11) is

$$\nabla^2\zeta + \frac{d}{dz} ln \left(U^2(z)\,\hat{\varrho}\,(z)\right)\frac{\partial\zeta}{\partial z} = -\frac{S(z)}{U^2(z)}\,\zeta \quad . \tag{5.13}$$

Eq. (5.13) is a good approximation to (5.11) if $(\nabla\zeta)^2 \ll 2\frac{\partial\zeta}{\partial z}$ and if z_0 may be replaced by z. The relative magnitude of $(\nabla\zeta)^2$ and $2\frac{\partial\zeta}{\partial z}$ depends on the height of the mountain. The streamline pattern due to a mountain of height 700 m is shown in Fig. 12. It is seen that $(\nabla\zeta)^2 \ll 2\frac{\partial\zeta}{\partial z}$, except for $z < 1$ km where $2\frac{\partial\zeta}{\partial z}$ is between two and three times as large as $(\nabla\zeta)^2$. It should therefore be expected that the main features of the flow are retained by cancelling the quadratic term.

The soundings show that usually $f \approx \frac{S}{U^2}$, and that S, the stability, is approximately constant in the troposphere. Now, since f is exponential in type in the lower troposphere, U is approximately an exponential function in this region. It has been mentioned above that also $\hat{\varrho}$ varies as an exponential function. Consequently the coefficient of the second term in (5.11) and (5.13) is approximately constant.

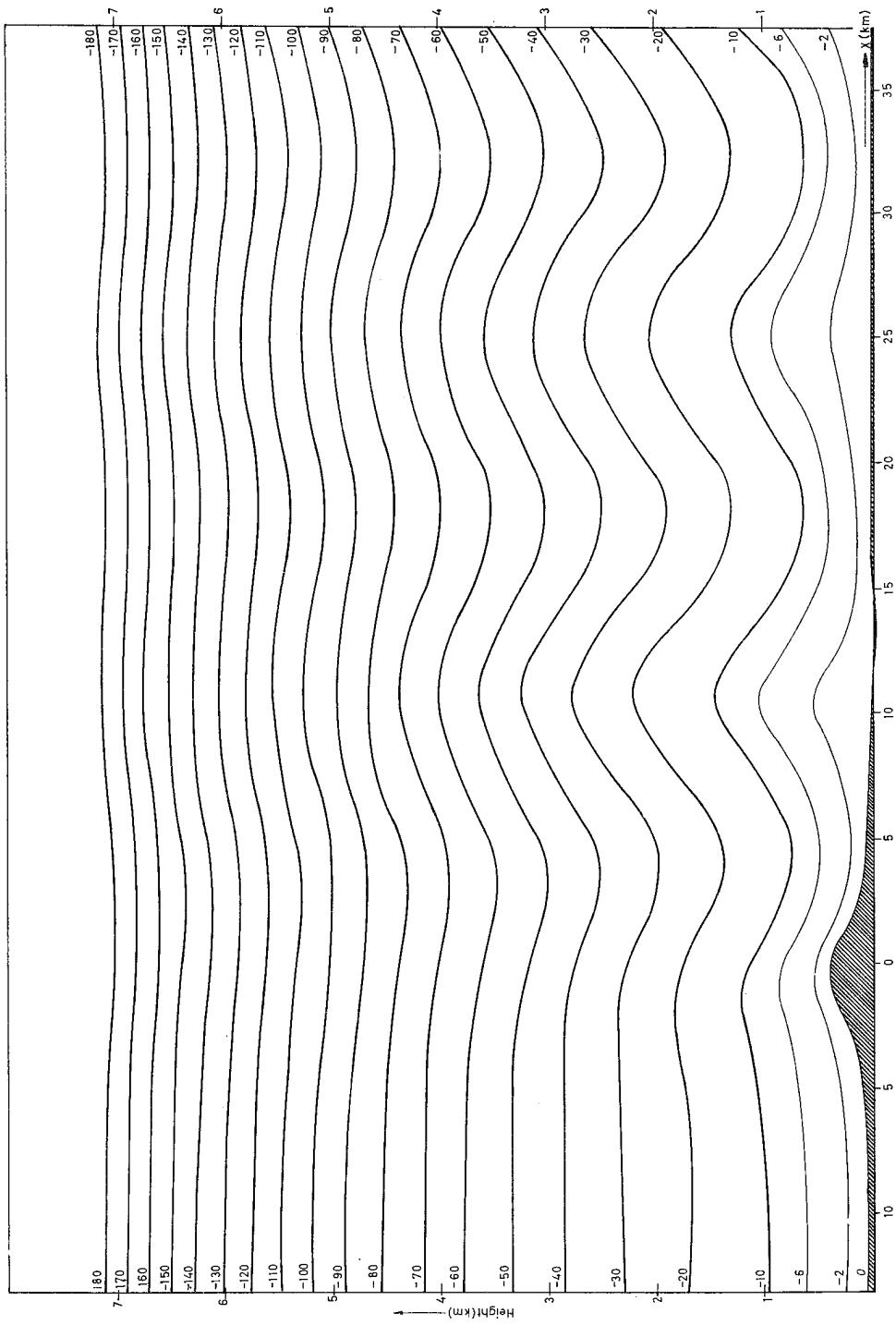

Figure 12. Streamlines due to a mountain of height 700 m. Units: $m^2 sec^{-1}$.

The term on the right in (5.11) and (5.13) is different mainly due to the difference between $U(z_0)$ and $U(z)$. Since U increases with height, $U(z)$ is greater than $U(z_0)$ at the crests and less at the throughs. Therefore, the term on the right in (5.13) is too small at the crests and too large at the troughs. This implies, which may be seen by expressing $\nabla^2\zeta$ by the vorticity, that the magnitude of the vorticity obtained by the linearized equation is too small at the crests and too large at the troughs. Consequently, the correct solution is sharper near the crests and flatter in the troughs than obtained by the linearized equation. It seems reasonable that this is the chief effect of replacing the non linear term on the right of (5.11) with the linear term on the right of (5.13).

The streamline pattern and rotor motion. The linearized solution for ω in the case of a mountain of form (3.4) is given by (5.3) and (5.4). The ω-field, and hence the streamline field, generated by the combined effect of a mountain peak with $H = 1$ km, $b = 2$ km and a valley centred at $x = 14.7$ km (corresponding to a wave length) and with $H = -0.1$ km and $b = 2$ km has been computed. Thus it is attained that the streamline

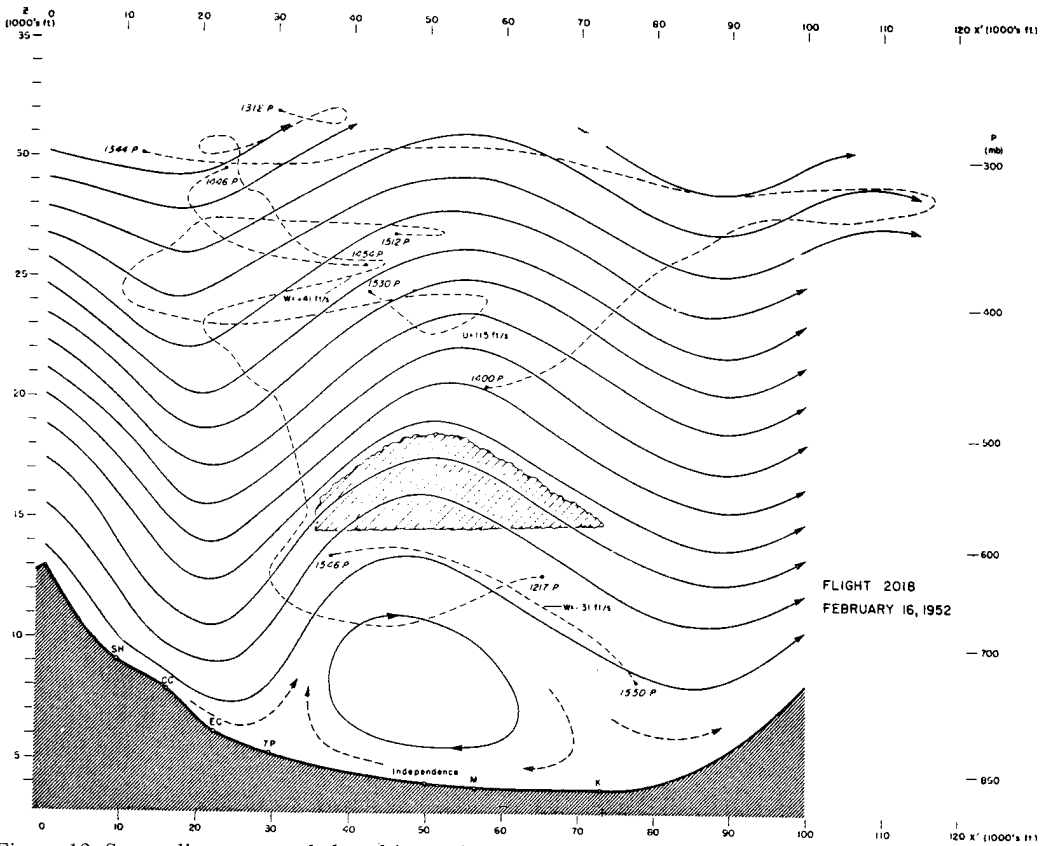

Figure 13. Streamline pattern deduced from observations of rotor flow in the Owens Valley on February 16, 1952, Sierra Wave Project.

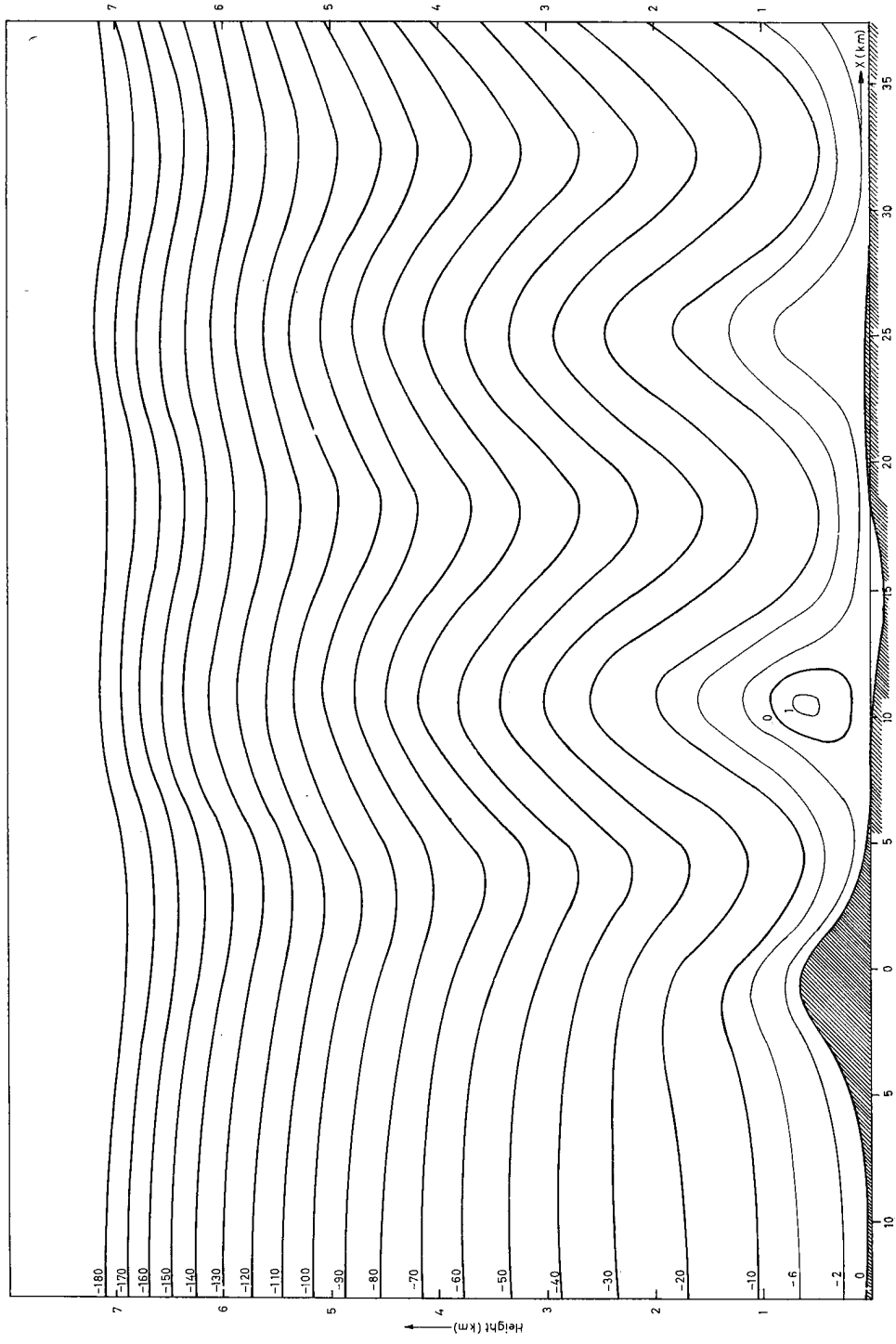

Figure 14. Streamlines due to a mountain of height 400 m. The distribution of wind and stability as in Fig. 12. Units: $m^2 sec^{-1}$.

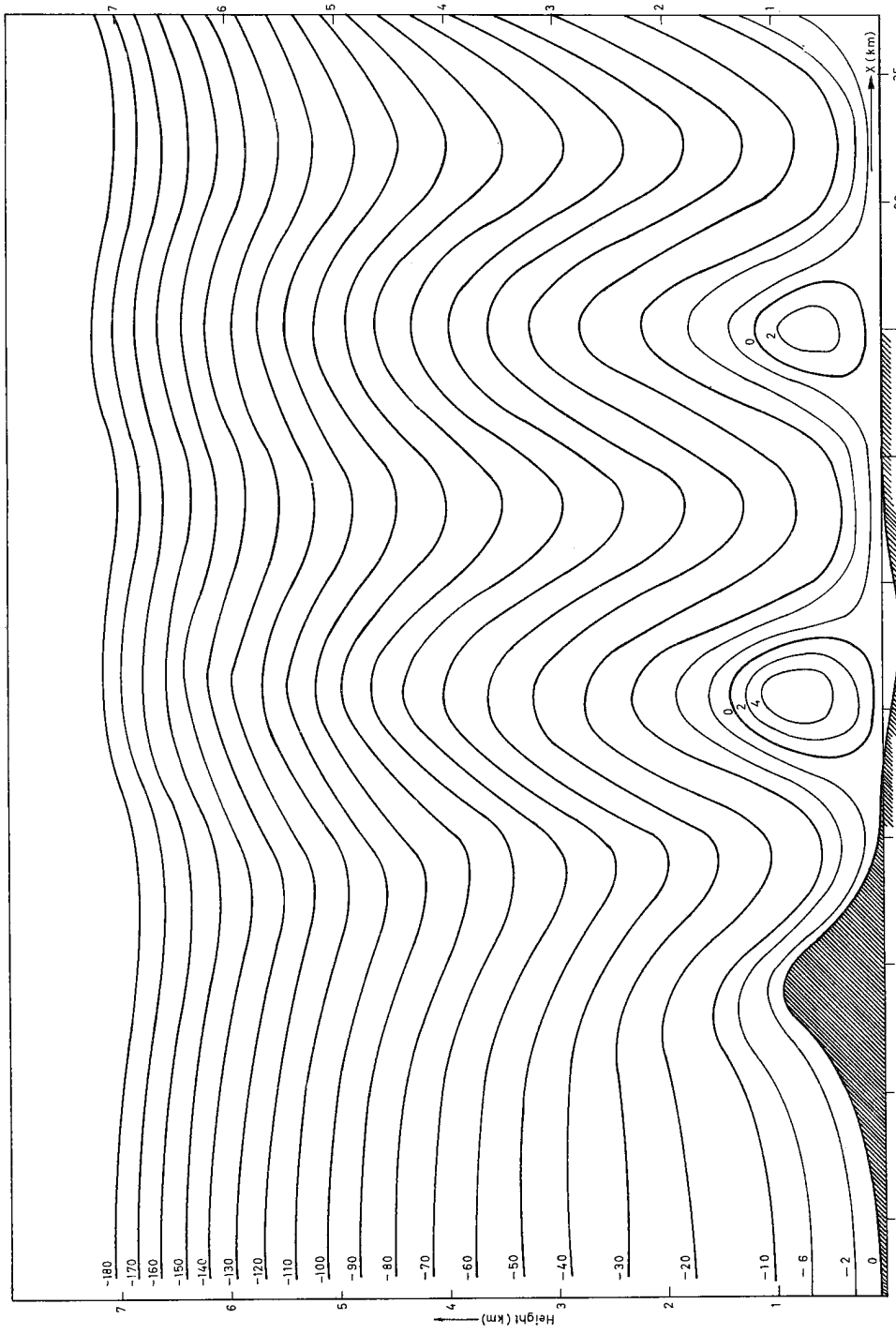

Figure 15. Streamlines due to a mountain of height 950 m. The distribution of wind and stability as in Fig. 12. Units: m^2sec^{-1}.

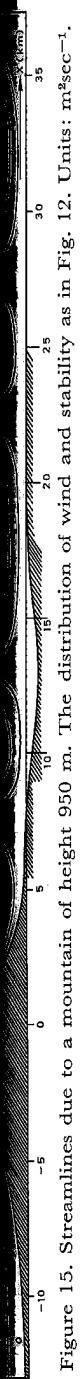

Figure 15. Streamlines due to a mountain of height 950 m. The distribution of wind and stability as in Fig. 12. Units: m^2sec^{-1}.

approaching the ground far upstream has the required form, i.e. a smooth profile consisting of one single ridge. As mentioned above the motion may be considered as generated by a mountain profile coinciding with this streamline, and is therefore not submitted to the restrictions implied in the linearization of the boundary conditions.

In the integrands (5.3) and (5.4) $\mathcal{J}_{iv}(\zeta)$ appears. This function is, so far as we know, not tabulated, and we have therefore applied the asymptotic expressions for Bessels functions of large order as well as large argument.

The streamline field obtained when $f(o) = f_1$, $c = c_1$ (f_1 and c_1 given in section 4) is shown in Fig. 12. It is noted that the height of the mountain is about 700 m. With the present distribution of wind and stability this mountain causes closed streamlines. Since the potential temperature is constant along a streamline, a closed streamline implies static instability and turbulence. It seems therefore very likely (LONG 1955) that these closed circulations correspond to the rotor motion observed for example in the Sierra Nevada region[1]. The streamline pattern observed in this region on February 16, 1957, the same day as the sounding applied here was observed, is displayed in Fig. 13. It should be mentioned that the sounding on which the model is based, was taken upstream in a valley between the coast mountains and Sierra Nevada. Therefore we have not taken into account the observed wind and stability below 1 km, i.e. $f(o)$ in the model corresponds to the observed $f(z)$ at 1 km. It turns out that choosing 1.7 km instead of 1 km gives complete agreement between observed and computed wave length.

The streamlines due to mountains of heights 400 m and 950 m are shown in Fig. 14 and Fig. 15, respectively. It is seen that no closed streamlines occur in the first case. In the second case, however, at least two sets of closed streamlines exist. With the present distribution of wind and stability the critical height for formation of closed streamlines is found to be 600 m.

Acknowledgement. The authors are indebted to Professor HØILAND, University of Oslo, for valuable discussions. This investigation has been sponsored by Norwegian Research Council for Science and the Humanities, and has in part been distributed as Report No. 4, 1958, Institute for Weather and Climate Research, Oslo.

APPENDIX

2A. Derivation of the differential equation. The equations of motion, the equation of continuity and the adiabatic equation may be written

$$\hat{\varrho}(Uu_x + U_z w) = -p_x \tag{2A.1}$$

$$\hat{\varrho}\, Uw_x = -p_z - g\varrho \tag{2A.2}$$

$$\hat{\varrho}\,(u_x + w_z) = -\frac{D}{dt}(\hat{\varrho} + \varrho) \tag{2A.3}$$

[1] Recently rotor motion in the atmosphere was also found by SCORER and KLIEFORTH (1959) applying a three-layer model.

$$\frac{D(\hat{\varrho}+\varrho)}{D(P+p)}=\frac{\delta}{g} \text{ or } \varrho=\frac{\delta}{g}p+\hat{\varrho}(\beta-\delta)\zeta \quad . \tag{2A.4}$$

The equations are linearized and the various symbols are defined in the list of symbols p. 29. $\frac{\delta}{g}=\frac{1}{s^2}$ (s the velocity of sound) may below with good approximation be considered as a constant. Introducing

$$u=\left(\frac{\hat{\varrho}(o)}{\hat{\varrho}(z)}\right)^{\frac{1}{2}}u^*,\ w=\left(\frac{\hat{\varrho}(o)}{\hat{\varrho}(z)}\right)^{\frac{1}{2}}\omega, \tag{2A.5}$$

$$\zeta=\left(\frac{\hat{\varrho}(o)}{\hat{\varrho}(z)}\right)^{\frac{1}{2}}\zeta^*,\ p=\left(\frac{\hat{\varrho}(z)}{\hat{\varrho}(o)}\right)^{\frac{1}{2}}p^*$$

and eliminating ϱ, the three first equations take the form

$$Uu_x^*+U_z\omega=-p^*_x \tag{2A.6}$$

$$U\omega_x+S\zeta^*=-p^*_z+\left(\frac{1}{2}\beta-\delta\right)p^* \tag{2A.7}$$

$$u^*_x+\omega_z+\left(\frac{1}{2}\beta-\delta\right)\omega=-\frac{\delta}{g}Up^*_x. \tag{2A.8}$$

Elimination of p^* and u^* and cancelling $\left(\frac{U}{s}\right)^2$ compared with unity leads to

$$\nabla^2\omega+\left(\frac{S}{U^2}-\frac{U_{zz}}{U}+(\beta-2\delta)\frac{U_z}{U}-\frac{1}{4}(\beta-2\delta)^2\right)\omega=0. \tag{2A.9}$$

Here $(\beta-2\delta)\frac{U_z}{U}-\frac{1}{4}(\beta-2\delta)^2$ are small compared to the other terms. Eq. (2A.9) may therefore be written

$$\nabla^2\omega+f(z)\omega=0 \tag{2A.10}$$

where

$$f(z)=\frac{S}{U^2}-\frac{U_{zz}}{U} \quad . \tag{2A.11}$$

Usually $\frac{S}{U^2}$ is the dominating term in this expression.

3A. Derivation of ω for section 3. The solution of Eq. (2.4) for the three layers in section 3 may be written

$$\begin{aligned}\omega_1&=A\sin\sqrt{f_1-k^2}\,z+B\cos\sqrt{f_1-k^2}\,z\\ \omega_2&=C\sin\sqrt{f_2-k^2}\,z+D\cos\sqrt{f_2-k^2}\,z\\ \omega_3&=E\mathcal{J}_{\nu_3}(\mathcal{Z}_3)\end{aligned} \tag{3A.1}$$

with the boundary condition at infinity implied. A, B, C, D and E are arbitrary constants to be determined by the boundary conditions. The other quantities are defined either in section 3 or in the list of symbols p. 29. According to section 2 the linearized boundary conditions are

$$\omega_1 = -\,a\,U(o)\,k\sin kx \qquad \text{at } z = o$$

$$\left.\begin{aligned} \omega_1 - \omega_2 &= o \\ \frac{d}{dz}(\omega_1 - \omega_2) &= o \end{aligned}\right\} \qquad \text{at } z = h_1 \tag{3A.2}$$

$$\left.\begin{aligned} \omega_2 - \omega_3 &= o \\ \frac{d}{dz}(\omega_2 - \omega_3) &= o \end{aligned}\right\} \qquad \text{at } z = h_2 \ .$$

It is here tacitly assumed that U_z is continuous at the interfaces. These equations determine the arbitrary constants, and the solution obtained for ω in layer n ($n = 1,2,3$) is

$$\omega_n = -\,a\,U(o)\,k\,\frac{\triangle_n(z,k)}{\triangle(k)}\sin kx \ . \tag{3A.3}$$

Here

$$\triangle(k) = \left(\mathcal{J}_{\nu_3}(\alpha_3)\cos\alpha_2 + \beta_2\mathcal{J}'_{\nu_3}(\alpha_3)\sin\alpha_2\right)\cos\alpha_1$$

and

$$-\,\beta_1\left(\mathcal{J}_{\nu_3}(\alpha_3)\sin\alpha_2 - \beta_2\mathcal{J}'_{\nu_3}(\alpha_3)\cos\alpha_2\right)\sin\alpha_1$$

$$\triangle_1(z,k) = \left(\mathcal{J}_{\nu_3}(\alpha_3)\cos(\alpha_2) + \beta_2\mathcal{J}'_{\nu_3}(\alpha_3)\sin\alpha_2\right)\cos\frac{h_1 - z}{h_1}\alpha_1$$

$$-\,\beta_1\left(\mathcal{J}_{\nu_3}(\alpha_3)\sin\alpha_2 - \beta_2\mathcal{J}'_{\nu_3}(\alpha_3)\cos\alpha_2\right)\sin\frac{h_1 - z}{h_1}\alpha_1 \ , \tag{3A.4}$$

$$\triangle_2(z,k) = \mathcal{J}_{\nu_3}(\alpha_3)\cos\frac{h_2 - z}{h_2 - h_1}\alpha_2 + \beta_2\mathcal{J}'_{\nu_3}(\alpha_3)\sin\frac{h_2 - z}{h_2 - h_1}\alpha_2 \ ,$$

$$\triangle_3(z,k) = \mathcal{J}_{\nu_3}(\mathcal{Z}_3) \ .$$

The following abbreviations are introduced

$$\alpha_1 = \sqrt{f_1 - k^2}\ h_1 \ , \quad \alpha_2 = \sqrt{f_2 - k^2}\,(h_2 - h_1) \ , \quad \alpha_3 = \mathcal{Z}_3(h_2) = \frac{\sqrt{f_3}}{c_3}e^{-c_3 h_1} \ , \tag{3A.5}$$

$$\beta_1 = \frac{h_1\alpha_2}{(h_2 - h_1)\alpha_1} \text{ and } \beta_2 = \frac{(h_2 - h_1)\,c_3\,\alpha_3}{\alpha_2} \ .$$

In the case of an arbitrary symmetrical mountain

$$\zeta = \int_0^\infty a(k)\cos kx\,dk \qquad \text{at } z = o \tag{3A.6}$$

ω_n may be written

$$\omega_n = -\,U(o)\,I\int_0^\infty a(k)\,k\,\frac{\triangle_n(z,k)}{\triangle(k)}\,e^{ikx}\,dk \tag{3A.7}$$

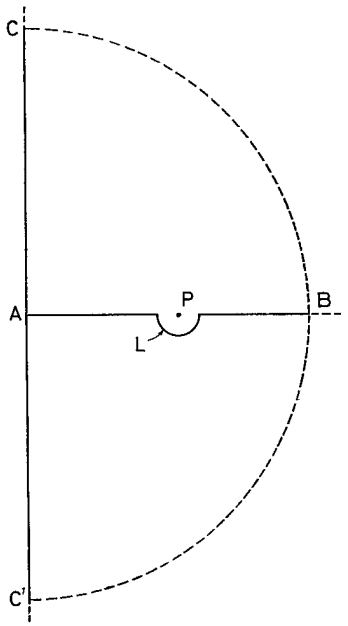

Figure 16. Path of integration.

where I indicates the imaginary part. If $\triangle(k) = o$ for any positive value of k, the integral does not exist. This difficulty is avoided, however, as pointed out in the introduction, by solving the problem as an initial value problem. It is then found that the improper integral (3A.7) is to be interpreted as an integral along the path of integration L shown in Fig. 16, corresponding to waves on the lee side only. In this figure P denotes one of the zeros of $\triangle(k)$.

A more appropriate form of (3A.7) is obtained by applying CAUCHY's theorem on the closed curves $ABCA$ for $x > o$ and $ABC'A$ for $x < o$. The dashed semi-circle indicates that the radius tends to infinity. It is then found that[1]

$$\omega = \omega_m + \omega_r \tag{3A.8}$$

where

$$\left.\begin{aligned} \omega_m &= U(o)\, I \int_0^\infty a(ik)\, k\, \frac{\triangle_n(z,ik)}{\triangle(ik)}\, e^{-kx}\, dk \\ \omega_r &= -2\pi\, U(o) \sum_k a(k)\, k\, \frac{\triangle_n(z,k)}{\frac{d}{dk}\triangle(k)} \cos kx \end{aligned}\right\} x > o \tag{3A.9}$$

$$\left.\begin{aligned} \omega_m &= -U(o)\, I \int_0^\infty a(ik)\, k\, \frac{\triangle_n(z,ik)}{\triangle(ik)}\, e^{kx}\, dk \\ \omega_r &= o \end{aligned}\right\} x < o \tag{3A.10}$$

The waves composing the sum in (3A.9) are the solutions of

$$\triangle(k) = o\ . \tag{3A.11}$$

4A. Derivation of ω for section 4. The solutions of Eq. (2.4) for the three layers in section 4 may be written

$$\begin{aligned} \omega_1 &= A\, \mathcal{J}_{\nu_1}(\mathcal{Z}_1) + B\, \mathcal{N}_{\nu_1}(\mathcal{Z}_1) \\ \omega_2 &= C \sin \sqrt{f_2 - k^2}\, z + D \cos \sqrt{f_2 - k^2}\, z \\ \omega_3 &= E\, \mathcal{J}_{\nu_3}(\mathcal{Z}_3) \end{aligned} \tag{4A.1}$$

[1] It is here and in (4A.8) assumed that $\triangle(k)$ has no complex zeros. The existence of such zeros corresponds to damped waves. In section 5 where the complete streamline field is required, these waves must be taken into account if they occur. It follows, however, from the theorem that Bessel functions of complex order and real argument have no zeros, that no such waves occur in the case studied in that section.

with the boundary condition at infinity implied. A, B, C, D and E are arbitrary constants and the other quantities are defined either in section 4 or in the list of symbols. The boundary conditions are the same as in 3A, and the solution obtained for ω in layer n ($n = 1,2,3$) is

$$\omega_n = a\,U(o)\,k\,\frac{\triangle_n(z,k)}{\triangle(k)}\sin kx \quad . \tag{4A.2}$$

Here

$$\begin{aligned}\triangle(k) = {} & \mu_1\left(-\mathcal{J}_{\nu_3}(\lambda_3)\sin\lambda_2 + \mu_2\mathcal{J}'_{\nu_3}(\lambda_3)\cos\lambda_2\right)\left(\mathcal{J}_{\nu_1}(\lambda_0)\mathcal{N}_{\nu_1}(\lambda_1) - \mathcal{J}_{\nu_1}(\lambda_1)\mathcal{N}_{\nu_1}(\lambda_0)\right) \\ & - \left(\mathcal{J}_{\nu_3}(\lambda_3)\cos\lambda_2 + \mu_2\mathcal{J}'_{\nu_3}(\lambda_3)\sin\lambda_2\right)\left(\mathcal{J}_{\nu_1}(\lambda_0)\mathcal{N}'_{\nu_1}(\lambda_1) - \mathcal{J}'_{\nu_1}(\lambda_1)\mathcal{N}_{\nu_1}(\lambda_0)\right)\end{aligned} \tag{4A.3}$$

and

$$\begin{aligned}\triangle_1(z,k) = {} & \mu_1\left(-\mathcal{J}_{\nu_3}(\lambda_3)\sin\lambda_2 + \mu_2\mathcal{J}'_{\nu_3}(\lambda_3)\cos\lambda_2\right)\left(\mathcal{J}_{\nu_1}(\mathcal{Z}_1)\mathcal{N}_{\nu_1}(\lambda_1) - \mathcal{J}_{\nu_1}(\lambda_1)\mathcal{N}_{\nu_1}(\mathcal{Z}_1)\right) \\ & - \left(\mathcal{J}_{\nu_3}(\lambda_3)\cos\lambda_2 + \mu_2\mathcal{J}'_{\nu_3}(\lambda_3)\sin\lambda_2\right)\left(\mathcal{J}_{\nu_1}(\mathcal{Z}_1)\mathcal{N}'_{\nu_1}(\lambda_1) - \mathcal{J}'_{\nu_1}(\lambda_1)\mathcal{N}_{\nu_1}(\mathcal{Z}_1)\right),\end{aligned} \tag{4A.4}$$

$$\triangle_2(z,k) = -\frac{2}{\pi\lambda_1}\left(\mathcal{J}_{\nu_3}(\lambda_3)\cos\frac{h_2-z}{h_2-h_1}\lambda_2 + \mu_2\mathcal{J}'_{\nu_3}(\lambda_3)\sin\frac{h_2-z}{h_2-h_1}\lambda_2\right),$$

$$\triangle_3(z,k) = -\frac{2}{\pi\lambda_1}\mathcal{J}_{\nu_3}(\mathcal{Z}_3) \quad .$$

The following abbreviations are introduced

$$\begin{aligned}&\lambda_0 = \mathcal{Z}_1(o) = \frac{\sqrt{f_1}}{c_1}\ ,\ \lambda_1 = \mathcal{Z}_1(h_1) = \lambda_0 e^{-c_1 h_1},\ \lambda_2 = \sqrt{f_2 - k^2}\,(h_2 - h_1)\ , \\ &\lambda_3 = \mathcal{Z}_3(h_2) = \frac{\sqrt{f_3}}{c_3}e^{-c_3 h_2},\ \nu_1 = \frac{k}{c_1}\ ,\ \nu_3 = \frac{k}{c_3}\ , \\ &\mu_1 = \frac{\lambda_2}{(h_2-h_1)\,c_1\lambda_1} \text{ and } \mu_2 = \frac{(h_2-h_1)\,c_3\,\lambda_3}{\lambda_2}\ .\end{aligned} \tag{4A.5}$$

In the case of an arbitrary symmetrical mountain

$$\zeta = \int_0^\infty a(k)\cos kx\,dk \qquad \text{at } z = o \tag{4A.6}$$

ω_n may be written

$$\omega_n = -\,U(o)\,I\int_0^\infty a(k)\,k\,\frac{\triangle_n(z,k)}{\triangle(k)}\,e^{ikx}\,dk \tag{4A.7}$$

where I indicates the imaginary part. By an analogous procedure as that applied in 3 A, it is found that

$$\omega = \omega_r + \omega_m \tag{4A.8}$$

where

$$\left.\begin{aligned} \omega_m &= U(o)\, I \int_0^\infty a(ik)\, k\, \frac{\triangle_n(z, ik)}{\triangle(ik)}\, e^{-kx}\, dk \\ \omega_r &= -\,2\pi\, U(o) \sum_k a(k)\, k\, \frac{\triangle_n(z,k)}{\dfrac{d\triangle(k)}{dk}} \cos kx \end{aligned}\right\} \quad x > o \tag{4A.9}$$

and

$$\left.\begin{aligned} \omega_m &= -\,U(o)\, I \int_0^\infty a(ik)\, k\, \frac{\triangle_n(z, ik)}{\triangle(ik)}\, e^{kx}\, dk \\ \omega_r &= o\ . \end{aligned}\right\} \quad x < o \tag{4A.10}$$

The waves composing the sum in (4A.9) are the solutions of

$$\triangle(k) = o. \tag{4A.11}$$

4B. The amplitudes in the lowest layer. Eq. (4A.3) may be simplified considerably for a wide range of k-values. $\mathcal{J}_{\nu_1}(\lambda_1)$ and $\mathcal{N}_{\nu_1}(\lambda_1)$ are oscillating functions of ν_1 being of the same order of magnitude when ν_1 is somewhat smaller than λ_1. If, on the other side, $\nu_1 > \lambda_1$, $\mathcal{N}_{\nu_1}(\lambda_1)$ increases exponentially whereas $\mathcal{J}_{\nu_1}(\lambda_1)$ decreases exponentially. Therefore, when ν_1 is somewhat larger than λ_1, $\mathcal{J}_{\nu_1}(\lambda_1)$ may be cancelled compared with $\mathcal{N}_{\nu_1}(\lambda_1)$. If, in addition, λ_0 is somewhat larger than λ_1, we obtain that $\mathcal{J}_{\nu_1}(\lambda_1)\,\mathcal{N}_{\nu_1}(\lambda_0)$ may be cancelled compared with $\mathcal{J}_{\nu_1}(\lambda_0)\mathcal{N}_{\nu_1}(\lambda_1)$, and, correspondingly, $\mathcal{J}'_{\nu_1}(\lambda_1)\mathcal{N}_{\nu_1}(\lambda_0)$ may be cancelled compared with $\mathcal{J}_{\nu_1}(\lambda_0)\,\mathcal{N}'_{\nu_1}(\lambda_1)$. As a rough rule the terms may be neglected (see for example JAHNKE and EMDE (1945)) if

$$\begin{aligned} &\nu_1 > \lambda_1 \\ &\lambda_0 > 1.5\lambda_1\ . \end{aligned} \tag{4B.1}$$

The approximation introduced by neglecting these terms is not good if ν_1 is very close to λ_1. The goodness of the approximation increases rapidly, however, when ν_1 increases relatively to λ_1.

(4B.1) may also be written

$$\begin{aligned} &k^2 > f_2 \\ &f_1 > 1.5^2 f_2 \approx 2.5 f_2\ . \end{aligned} \tag{4B.2}$$

In the actual case $\lambda_0 = 5\lambda_1$ ($f_1 = 25 f_2$), and Eq. (4A.11) reduces for $k^2 > f_2$ (i.e. for wave lengths less than 25 km) to

$$G(k)\, \mathcal{J}_{\nu_1}(\lambda_0) = o \tag{4B.3}$$

where

$$\begin{aligned} G(k) = \mu_1 \mathcal{N}_{\nu_1}(\lambda_1) &\left(-\,\mathcal{J}_{\nu_3}(\lambda_3) \sin\lambda_2 + \mu_2 \mathcal{J}'_{\nu_3}(\lambda_3) \cos\lambda_2\right) \\ &- \mathcal{N}'_{\nu_1}(\lambda_1) \left(\mathcal{J}_{\nu_3}(\lambda_3) \cos\lambda_2 + \mu_2 \mathcal{J}'_{\nu_3}(\lambda_3) \sin\lambda_2\right)\ . \end{aligned} \tag{4B.4}$$

Correspondingly, for $\nu_1 > \lambda_1$ and $\mathcal{Z}_1 > 1.5\lambda_1$ (i.e. $z < 5$ km in the actual case) $\triangle_1(z,k)$ simplifies to

$$\triangle_1(z,k) = G(k)\,\mathcal{J}_{\nu_1}(\mathcal{Z}_1), \tag{4B.5}$$

approximately. Therefore, as to the wave motion near the ground (i.e. in the actual case below 5 km) $G(k)$ drops out. The part of the wave motion near the ground composed of waves for which $k^2 > f_2$ may thus be obtained from a one-layer model with $f(z)$ varying as an exponential function.

LIST OF SYMBOLS

a, $a(k)$	Fourier cosine transform of the mountain profile.
b	defined by Eq. (3.4)
c	defined by Eq. (5.1). (c_1 and c_3 are defined in sections 3 and 4).
$f(z)$	$= \frac{S}{U^2} - \frac{U_{zz}}{U}$
g	acceleration of gravity
H	defined by Eq. (3.4)
$\mathcal{J}_\nu(\mathcal{Z})$	Bessel function of first kind
k	wave number
$N_\nu(\mathcal{Z})$	Bessel function of second kind
P	pressure in the undisturbed motion
p	perturbation pressure
S	$= g(\beta - \delta) = \frac{g(\gamma_d - \gamma)}{T}$, stability
s	velocity of sound
T	temperature
U	basic velocity
$U + u$	total horizontal velocity
w	vertical velocity
x,z	Cartesian coordinates, z vertical. Subscripts x,z denote differentiation
z_0	height of a streamline in the undisturbed motion
$\mathcal{Z}$	$= \mathcal{Z}(z) = \frac{\sqrt{f(o)}}{c} e^{-cz}$
β	positive constant defined in connection with $\hat{\varrho}$
γ	actual lapse rate
γ_d	dry adiabatic lapse rate
δ	$= \frac{g}{s^2}$, defined by Eq. (2A.4)
ζ	vertical displacement of a streamline
λ_0	$= \mathcal{Z}(o)$

ν $= \dfrac{k}{c}$

ϱ perturbation density

$\hat{\varrho}$ $= \hat{\varrho}(z) = \hat{\varrho}(o)e^{-\beta z}$, density in the undisturbed motion

ω $= we^{-\frac{\beta}{2}z}$

ω_r the part of ω being harmonic waves

ω_m $= \omega - \omega_r$

∇^2 $= \dfrac{\partial^2}{\partial x^2} + \dfrac{\partial^2}{\partial z^2}$

REFERENCES

ELIASSEN, E., and E. C. KLEINSCHMIDT Jr., 1957: Dyn.Met., *Handbuch der Physik*, **48**, Berlin.

ELIASSEN, E., and E. PALM, 1954: *Inst. for Weather and Climate Research, Publ. No. 1*, Oslo.

GEORGII, W., 1956: *Flugmeteorologie*, 2., neubearb. Aufl., Frankfurt am Main.

HESSTVEDT, E., 1959: *Geof. Publ.* **20**, No. 10, Oslo.

HOLMBOE, J., and H. KLIEFORTH, 1957: *Sierra wave project*, Final report, March 1957 (Dept. of Met., Univ. of California).

HØILAND, E., 1951: *Sierra wave project*, Appendix A, Fifth progress report (Dept. of Met., Univ. of California).

JAHNKE, E., and F. EMDE, 1945: *Tables of functions*, New York.

KELVIN, Lord, 1886: *Phil. Mag.* (5) **22**, 353–373, 445–452, 517–530.

LONG, R. R., 1953: *Tellus* **5**, p. 42.

— 1955: *Ibid* **7**, p. 341.

LYRA, G., 1943: *Zeit. f. ang. Math.u.Mech.* **23**, 1–28.

MURGATROYD, R. J., 1957: *Quart. J. R. Met. Soc.* **83**, p. 417.

PALM, E., 1953: *Astroph. Norv.* **5**, No. 3, Oslo.

— 1958: *Geof. Publ.* **20**, No. 3, Oslo.

QUENEY, P., 1947: *Dept. of Met. of the Univ. of Chicago, Misc. reports* No. 23.

RAYLEIGH, Lord, 1883: *Proc. London Math. Soc.* **15**, 69–78.

SAWYER, J. S., 1959: *Quart. J. R. Met. Soc.* **85**, p. 31.

SCORER, R. S., 1949: *Ibid*, **75**, p. 41.

SCORER, R. S. and H. KLIEFORTH, 1959: *Ibid.* **85**, p. 131.

WURTELE, M., 1953a: *Sierra wave project, Scientific report* No. 3 (Dept. of Met., Univ. of California).

— 1953b: *Sierra wave project*, Progress report (Dept. of Met., Univ. of California).